Damage depth profile in α-Al2O3 induced by swift heavy ions

A. Ribet, J-G. Mattei, I. Monnet, C. Grygiel

Version of Record: https://www.sciencedirect.com/science/article/pii/S0168583X19301089
Manuscript_986477d3f6a7fc73ed86eceb85441dca

Damage depth profile in α-Al_2O_3 induced by swift heavy ions

A. Ribet, J-G. Mattei, I. Monnet and C. Grygiel*

Normandie Univ, ENSICAEN, UNICAEN, CEA, CNRS, CIMAP, 14000 Caen, France

Abstract

Structural modifications of aluminium oxide induced by swift heavy ion irradiation are investigated. (0001)-Al_2O_3 single crystals have been irradiated at room temperature along the *c*-direction by 92 MeV Xe^{23+} with fluences up to $1.2x10^{15}$ ions/cm^2. High resolution and in-plane X-Ray diffraction is mainly used to characterize samples with various sensitivities to the surface and to the irradiated depth. As function of fluence the mechanisms of structural modifications are investigated. Different evolutions of the *c*-parameter (parallel to ion beam) and the *a*-parameter (perpendicular to ion beam), affected by irradiation in the MeV range, are observed. 2D maps around (0006)-reflection indicate a clear broadening on 2Θ axis with the formation of new contributions which are due to tensile strain induced by irradiation. In the damage profile, by combining with RBS/C and TEM results, we suggest that the *c*-parameter is larger near the surface and decreases gradually with depth. In addition, the damage profile evidences an increase of damaged depth as function of the fluence which occurs before saturation linked to the formation at the surface of an amorphous layer.

Keywords: Al_2O_3, ion irradiation, XRD, damage profile

* Corresponding author: *grygiel@ganil.fr* (C. Grygiel)

Introduction

The aluminium oxide α-Al_2O_3 has been studied a lot since some years as well in polycrystals as in single crystals and under different ion energy conditions (inelastic or elastic ranges) [1-3]. Under swift heavy ion (SHI) irradiation, Al_2O_3 behavior is a bit different compared to other insulators as it is intermediary between an amorphizable and a non-amorphizable material. Above a threshold in terms of electronic stopping power (S_{eth} ~ 10 keV/nm), Al_2O_3 exhibits discontinuous tracks and amorphization after track overlap by the surface and at high fluence [4-6]. In polycrystals it was indeed previously reported that along the ion path, first an amorphous layer is observed beneath the surface, then an intermediary damaged layer, and finally very deep a free-defect region [6,7]. Grazing incidence X-Ray diffraction (GI-XRD) has shown on these pellets that the crystalline phase exhibits sensitivity to SHI by the formation of long range and short range strains and domain size decrease for example. However GI-XRD provides only average information on the diffracting grains, and in order to get a precise view of damage depth profile, high resolution XRD (HR-XRD) has been performed on Al_2O_3 single crystals irradiated by SHI. In contrast to previous studies using the XRD on single crystals by measuring only the out-of-plane reflection [8,9], the idea of the current paper is to show how the structural properties of sapphire are affected by measuring six different crystallographic directions. In this way, we aim to suggest how the damaging occurs along the ion path in the case of SHI by establishing a strain profile. A particular care is also to look at if strain relaxation will take place along the ten of micrometers of the ion path.

Experimental

Sapphire single crystal samples ((0001)-orientation, 500 µm thick) are irradiated with 92 MeV Xe^{23+} ions at normal incidence and room temperature. Irradiation experiments are performed at IRRSUD beam line of the GANIL accelerator facility (Caen, France). Samples of dimensions 5 mm x 5 mm are irradiated homogeneously by a scanned ion beam. The samples are fixed on the irradiation holder by a conductive carbon tape which is an electrical conductor. The ion flux is kept to a low value (2-5x10^9 ion.cm^{-2}.s^{-1} corresponding to less than 2 W) to avoid macroscopic sample heating and the resulting effects. Using the Kinchin and Pease option of SRIM code [10], the ion energy losses are calculated for 92 MeV ^{129}Xe in sapphire with theoretical density (4 g/cm^3) and displacement energies of 20 eV for Al and 50 eV for O. At this energy, the electronic regime is predominant on most of the ion beam path. At the surface the value of the electronic stopping power S_e is 21 keV/nm well above the S_e threshold for track formation. The S_e value decreases along the ion path until an inversion of energy deposition processes, where nuclear stopping power S_n rises slightly at 7-8 µm near the end of the projected range (R_p=8.4±0.1 µm).

XRD measurements are carried out with a Bruker D8 Discover equipment using a parallel beam geometry with a Göbel mirror for K_α copper radiation source. The diffractometer has an

Euler cradle allowing four-circle movements where sample and detector are rotated. 2θ is the diffraction angle between the incident beam and the detector, ω the incident angle between x-ray source and sample surface, chi the inclination angle (0-90°) between the crystallographic plane and the sample surface, and phi the azimuthal angle (0-360°) or the sample rotation on itself. Moreover, symmetric geometry uses $2\theta = 2\omega$ condition while asymmetric uses $2\theta \neq 2\omega$. Several reflections are recorded with different optics and geometries to study material behavior in many reciprocal space directions. First, triple-axis geometry using a 2-bounce Ge-220 monochromator, an analyser crystal and a scintillation detector enables high resolution symmetric patterns (0006 reflection), symmetric skew patterns ($10\bar{1}4$, $11\bar{2}3$, $21\bar{3}4$ reflections, chi≠0 and chi<90°), asymmetric patterns ($01\bar{1}8$(-)) reflections with (-) meaning "grazing" incident beam, chi=0°) and 2D maps. 2D maps are obtained by taking a series of 2θ_ω patterns (± 0.5° around the reference position) at successive ω values (± 0.5° around the reference position). Sketches of the geometries are seen ref. [11]. These five reflections allow probing the irradiated material very deep even after the projected range. Table 1 displays the different characteristics of each reflection observed where depth values are measured taking 90% of I/I_0 intensity ratio, the material density and a mass attenuation coefficient of 31.5 cm^2/g. Also using in-plane geometry (chi=90°) with primary slits, equatorial slits (0.1°) and a LYNXEYE detector in 0D, ($11\bar{2}0$) reflection is recorded with an incident grazing angle of around 0.3° probing sample to 240±40 nm where the S_e is the highest. Indeed the analysis of all these reflections allow to observe all damaged area, from the surface up to the projected range, and even deeper where the material remains virgin and non-irradiated. For the 2D map representations, the viewers are DxTools [12] for the reciprocal space or Bruker Diffrac Leptos software for the direct space. Leptos is also used to simulate the XRD patterns including contributions of irradiated material showing a damage profile.

Results and discussion

To get a general view of structural modifications induced in sapphire under 92 MeV Xe, 2D maps are recorded for four reflections at different ion fluences up to high value ($1.2x10^{15}$ ions/cm²), Fig. 1 shows these maps in the direct space. The dotted lines on the maps help to observe the contribution of the non-irradiated layer or virgin layer of Al_2O_3 samples, called the reference peaks. On the virgin sample and for all the reflections, fine and intense reflections are observed with streaks formation due to optics (monochromator and analyzer). It shows the high crystalline quality of the initial virgin sample. When the fluence increases up to $1.2x10^{15}$ ion/cm^2, a broadening of the reflections is noticed. On ω axis, the broadening means a slight tilt of diffracting domains and a slight increase of mosaicity along the *c*-direction of ± 0.02° at maximum. Additionally, a large broadening is observed on 2Θ axis with the formation of new contributions at relatively high intensities which are inevitably created by the ion irradiation. These 2Θ reflections are always extended towards low diffraction angles, meaning that tensile strain is induced by irradiation. Such broadening was already mentioned for the (0006) reflection measured with low resolution setups [8,9]. Otherwise the 2D maps show a lower variation of the lattice strains for the ($10\bar{1}4$), ($11\bar{2}3$) and

$(21\bar{3}4)$ reflections. Moreover next to these large intensities, diffuse signal or scattering appears at higher angles for high fluences, which means compressive disorder and amorphous area formation. Thus high resolution symmetric measurements are performed in the center of each reflection (ie large intensities) to analyze the behaviour under irradiation with more accuracy.

Fig. 2 shows HR patterns for the (0006) reflection for several fluences. At higher angles (around 41.66°), fine reference peaks are clearly observed whatever the level of damage which is consistent with the X-ray absorption in Al_2O_3 and the depth probed by X-rays (32.5±0.5 µm) well above the R_p (8.4±0.1 µm) implying a huge ratio of non-irradiated matter. In addition, Fig. 2 reveals with a good resolution the aforementioned contributions close to reference peaks shifting towards low 2θ angles as function of the fluence. Furthermore, the HR patterns highlight that the peak corresponding to the maximum tensile strain (at the lowest angle on each pattern) shifts to lower angle or higher strain at each step of the fluence increase. This gap between the reference peak and the peak of maximum strain increases up to a full strain value (0.86±0.10% at $2x10^{14}$ ion/cm^2) and thereafter decreases or seems to relax at the highest fluence ($1.2x10^{15}$ ion/cm^2). Thus, strain according to the *c*-parameter and parallel to the ion beam increases with fluence and corresponds to lattice expansion in this direction. The evolution of the maximum strain as function of fluence has been fitted by a Poisson law using a sigmoidal function to extract the cross section of the damaged cylinder and the kinetics of the damaging. A single impact kinetics better fits the strain evolution (R^2=0.98) for an ion track radius of around 2.4±0.8 nm, whose track radius is consistent with those of amorphization requiring the overlap of at least two tracks [6]. As the amorphization process requires inelastic energy losses above a threshold, the strain formation is also at least partially linked to the electronic process. In addition, as several contributions are observed between the reference and maximum peaks, we consider that a gradient of strain is formed during irradiation and the number of contributions increases as function of the fluence. Oscillations are also noticed at $1.2x10^{15}$ ions/cm^2 meaning interferences due to different diffracting layers certainly in terms of disorder or density, which are not further detailed.

In order to observe if the crystallographic direction perpendicular to ion beam is affected, two others reflections are measured: one in asymmetric configuration the $(01\bar{1}8(-))$ reflection and one in in-plane configuration the $(11\bar{2}0)$ reflection. Both are benefiting of grazing incidence of the X-Ray beam allowing sensitivity to the full irradiated layer with 24±1 µm probed for $(01\bar{1}8(-))$ and sensitivity to irradiated surface layer 240±40 nm for the in-plane $(11\bar{2}0)$. Fig. 3 shows 2D maps of the $(01\bar{1}8(-))$ reflection for the virgin and the $1.2x10^{15}$ ions/cm^2 samples, where Q_z value is directly linked for this reflection to *c*-parameter through the formula $Q_z=8*2\pi/c$ whereas Q_x axis is linked to *a*-parameter with the formula $Q_x=4\pi/(a\sqrt{3})$. Fine and intense reflection can be observed on the virgin sample with streaks coming from optics. When the fluence increases, several phenomena are noticed: formation of diffuse scattering and on the intense peaks broadening along Q_z axis and almost no change on Q_x axis (neither width nor position). Moreover, the 2D map at $1.2x10^{15}$ ions/cm^2 shows the same evolution than previously observed: an intense reference peak (with same value of Q_x and Q_z than the virgin sample), and a strain gradient which extends to a much lower value of Q_z (ie around

Q_z=3.84 or c=13.089 Å) corresponding to the maximum of strain. Even at this high fluence, the 2D map does not evidence besides the diffuse signal any variations of the intense peaks on Q_x axis apart from a very small broadening. This highlights that there is almost no parameter variation along the a-axis whereas ion beam effect is well observed along c-axis, at least in the material depth probed during the $(01\bar{1}8(-))$ measurement. In order to be sensitive to the irradiated layer in surface where mainly inelastic energy is deposited, the $(11\bar{2}0)$ in-plane reflection is measured as function of the irradiation fluence. The evolution of patterns on 2Θ axis is not represented as very few modifications of the peak are observed. However, the Fig. 4 illustrates the strain $\varepsilon_a=a_i-a_0/a_0$ of the a-parameter extracted from the $(11\bar{2}0)$ position. The uncertainty bars reveal the low resolution of this geometry on the contrary to all previous measurements. Very slight fluctuation around the virgin value is observed even up to high fluence. The highest fluences of $2x10^{14}$ and $1.2x10^{15}$ ions/cm^2 are not represented because the reflections were not measurable, which is consistent with the amorphization from the surface (amorphous depths measured by TEM about 500 nm and 3200 nm respectively). Regarding the intense peaks corresponding to the crystalline α-Al_2O_3 phase, we then conclude that no evolution of the in-plane lattice parameter is observed in the perpendicular direction to the ion beam. Thus (0001)-Al_2O_3 single crystals irradiated with SHI (92 MeV Xe) exhibit whatever the location along the 8.4±0.1 µm of ion path only tensile strain parallel to ion beam. Due to the effect of substrate inducing biaxial stress [13], where the substrate in our case is the non-irradiated material present beyond the R_p, no variation of the lattice parameter is observed in the orthogonal direction. Even if substrate effect was already reported for irradiated crystals at low ion energy [14,15], this result at high ion energy was not obvious as a relaxation of biaxial stress could have taken place along the ten micrometers of R_p, which is not the case.

From now, the purpose is to establish a depth profile of disorder induced in sapphire as function of the fluence. Simulations of diffraction patterns are done for irradiated sapphire containing signals from the non-irradiated layer, the maximum strain layer and all contributions of layers with intermediate strains, whose value and thickness vary with ion fluence. Hypotheses on layer location are done to simulate the depth profile as for a layer of given strain and thickness the position of the layer in depth could be slightly exchanged with another layer without significant change of X-Ray pattern. The location of the non-irradiated layer is obviously beyond the projected range. Considering the location of the maximum strain, at the surface or buried deep, we have previously concluded that the strain formation is partially linked to inelastic energy losses which are maximum at the entrance in the material and decrease continuously along the ion path. Indeed, the literature about Al_2O_3 single-crystals reports studies done with RBS-C experiments on sapphire irradiated in similar conditions and for which the level of damage increases with fluence and from the surface [8,16]. It is also reported through TEM observations that the amorphous layer, induced by S_e deposition, grows by the surface at high fluence with a maximum of damage at its border amorphous/crystalline [6,7,9]. We thus consider that the strain gradient exhibits a maximum level in the layer near the surface, the strain level decreases gradually through a certain number of layer contributions along the ion path down to a level strain free, ie the non-irradiated layer. Using such a stacking of layers with various levels of strain, for the sample irradiated at $2x10^{13}$ ions/cm^2 the (0006) pattern is simulated (insert of Fig. 5) using Leptos

and compared to the experimental curve. A good agreement is observed between the two curves. In the simulation several layers are used by adjusting for each of them thickness and *c*-parameter as detailed Fig. 5 as function of depth. Such simulation is performed for the different fluences. The layer number required for the better adjustment of the simulation increases as function of fluence. The simulations evidence that the *c*-parameter of the maximum strain layer, located at the surface or at the border amorphous/crystalline, increases as function of the fluence up to a full value about 13.107±0.005 Å at $2x10^{14}$ ions/cm^2. The maximum *c*-parameter for $1.2x10^{15}$ ions/cm^2 is lower than for $2x10^{13}$ and $2x10^{14}$ ions/cm^2 due to the amorphization at the surface (where we supposed to be located the full strain), saturation of defects and material relaxation. The shift from the surface (depth=0) corresponds to the amorphous layer whose thickness grows with fluence, where no lattice parameter can be extracted. The Fig. 5 also evidences the progressive decrease of the tensile strain level as function of the depth along the ion path. By summing all the layer thicknesses (amorphous and strained), the damaged depth increases with fluence from around 1600 nm for $5x10^{12}$ ions/cm^2 up to 8450 nm for $1.2x10^{15}$ ions/cm^2 which is in the order of the projected range. This means that the tensile strain or unit-cell swelling induced along the ion path is not only due to electronic stopping power but also nuclear process as modification of lattice parameter is noticed all along the projected range, even if the maximum strain is located where the S_e is dominant and S_n low. Swelling in alumina is already reported to be induced by S_n or S_e or S_n and S_e as in polycrystals where both energy losses contribute to unit-cell swelling [6,17-19]. These results highlight that the evolution of Al_2O_3 behaviour as function of ion fluence is complex. This is not just a damage accumulation induced by latent tracks as soon as we are above a threshold, but the maximum strain grows with fluence increase, the damaged depth increases as well, and amorphization takes place by the surface. Such depth profiles of structural properties bring in this way new inputs to the understanding of Al_2O_3 under SHI.

Conclusions

In this work, sapphire single crystals have been irradiated with 92 MeV Xe^{23+} ions at different fluences at the GANIL facility. HR and in-plane X-Ray diffraction experiments were performed to analyze the behaviour of α-Al_2O_3 under ion irradiation. Two signals have been measured: one diffuse observed at high fluence attributed to the radiation induced amorphous phase and one intense for the crystalline phase showing with ion fluence a progressive damaging described in the current study. A tensile strain is measured in the out-of-plane direction, parallel to the ion beam, whereas almost no variations are measured in the orthogonal direction to the ion beam. This highlights the significant effect of the non-irradiated layer, present deeper than the projected range, and still inducing a compressive biaxial stress along the ten of micrometers of ion path. To suggest a damage depth profile, hypotheses using data of RBS-C and TEM have been done to help simulation of X-Ray patterns considering that the layer of maximum strain is located at the amorphous/crystalline border. The profile emphasizes that the maximum strain grows with fluence increase, the damaged depth increases as well, while amorphization takes place by the surface and grows with fluence. It has been discussed that both electronic and nuclear contributions are required

for such strain evolution. The characterization method carried out in the current study can be applied in the future to others crystalline systems to get comprehensive overview on structural properties evolution under swift heavy ion irradiation.

Acknowledgements

The experiments were performed at the IRRSUD beamline of the Grand Accélérateur National d'Ions Lourds (GANIL), Caen, France. The authors thank the CIMAP staff, especially T. Madi, the CIRIL platform staff, the GANIL technical staff and the overall administrative staff. The authors would like to thank H. Lebius, E. Balanzat (CIMAP), A. Debelle (CSNSM, France) and A. Boulle (SPCTS, France) for fruitful discussions. This work was partially supported by the ANR funding "Investissements d'avenir" ANR-11-EQPX-0020 and ANR10-LABX-09-01 LabEx EMC3, the FEDER and by the Region Basse-Normandie.

References

[1] S. J. Zinkle, J. Nucl. Mat. 219 (1995) 113.
[2] B. Canut, A. Benyagoub, G. Marest, A. Meftah, N. Moncoffre, S. M. M. Ramos, F. Studer, P. Thevenard , M. Toulemonde, Phys. Rev. B 51 (1995) 12194.
[3] V.A. Skuratov, S.J. Zinkle, A.E. Efimov, K. Havancsak, Nucl. Instr. Meth. B 203 (2003) 136.
[4] G. Szenes, J. Nucl. Mat. 336 (2005) 81.
[5] V. A. Skuratov, J. O'Connell, N.S. Kirilkin, J. Neethling, Nucl. Instr. Meth. B 326 (2014) 223.
[6] C. Grygiel, F. Moisy, M. Sall, H. Lebius, E. Balanzat, T. Madi, T. Been, D. Marie, I. Monnet, Act. Mat. 140 (2017) 157.
[7] T. Aruga, Y. Katano, T. Ohmichi, S. Okayasu, Y. Kazumata, Nucl. Instr. Meth. B 166 (2000) 913.
[8] A. Kabir, A. Meftah, J.P. Stoquert, M. Toulemonde, I. Monnet, M. Izerrouken, Nucl. Instr. Meth. B 268 (2010) 3195.
[9] N. Okubo, N. Ishikawa, M. Sataka, S. Jitsukawa, Nucl. Instr. Meth. B 314 (2013) 208.
[10] J.F. Ziegler, J.P. Biersack, U. Littmark, in: J.F. Ziegler (Ed.), The Stopping and Range of Ions in Solids, vol. 1, Pergamon, New York, 1985 (Chap. 8).
[11] M.A. Moram, M.E. Vickers, Rep. Prog. Phys 72 (2009) 036502
[12] A. Boulle, J. Appl. Cryst. 50 (2017) 967.
[13] J.-D. Kamminga, Th. H. de Keijser, R. Delhez, E. J. Mittemeijer, J. Appl. Phys. 88 (2000) 6332.
[14] A. Debelle, A. Declémy, L. Vincent, F. Garrido, L. Thomé, J. Nucl. Mat. 396 (2010) 240.
[15] A. Debelle, A. Declémy, Nucl. Instr. Meth. B 268 (2010) 1460.
[16] A. Kabir, A. Meftah, J.P. Stoquert, M. Toulemonde, I. Monnet, Nucl. Instr. Meth. B 266 (2008) 2976.
[17] G.P. Pells and M.J. Murphy, J. Nucl.Mater. 191-194 (1992) 621.
[18] G.P. Pells, J.Am. Ceram. Soc. 77 (1994) 368.
[19] A. Kabir, A. Meftah , J.P. Stoquert , M. Toulemonde , I. Monnet , M. Izerrouken Nucl. Instr. Meth. B 268 (2010) 3195.

Figure captions

Fig. 1: 2D maps for four reflections of sapphire irradiated with 92 MeV Xe. 2θ axis is from left to right, ω axis from bottom to top, the same scale is used on all the maps.

Fig. 2: HR-XRD patterns for the (*0006*) reflection as function of the ion fluences (in Xe/cm²). Patterns are shifted manually and arbitrarily for a better visibility.

Fig. 3: Reciprocal space maps of the reflection ($01\bar{1}8$(-)) as function of 92 MeV Xe fluence.

Fig. 4: Strain of *a*-parameter as function of 92 MeV Xe fluence.

Fig. 5: *c*-parameter evolution as function of the depth and ion fluence (Xe/cm²). The shift from the surface (depth=0) corresponds to the amorphous layer whose thickness grows with fluence, where no lattice parameter can be extracted. Insert: HR-XRD and simulated patterns for the (*0006*) reflection at $2x10^{13}$ ion/cm². The black line is the experimental HR pattern and the red line is the simulation.

Table

Table 1: Characteristics of measured reflections: Bragg angle (2θ), chi inclination angle and the corresponding probed depth.

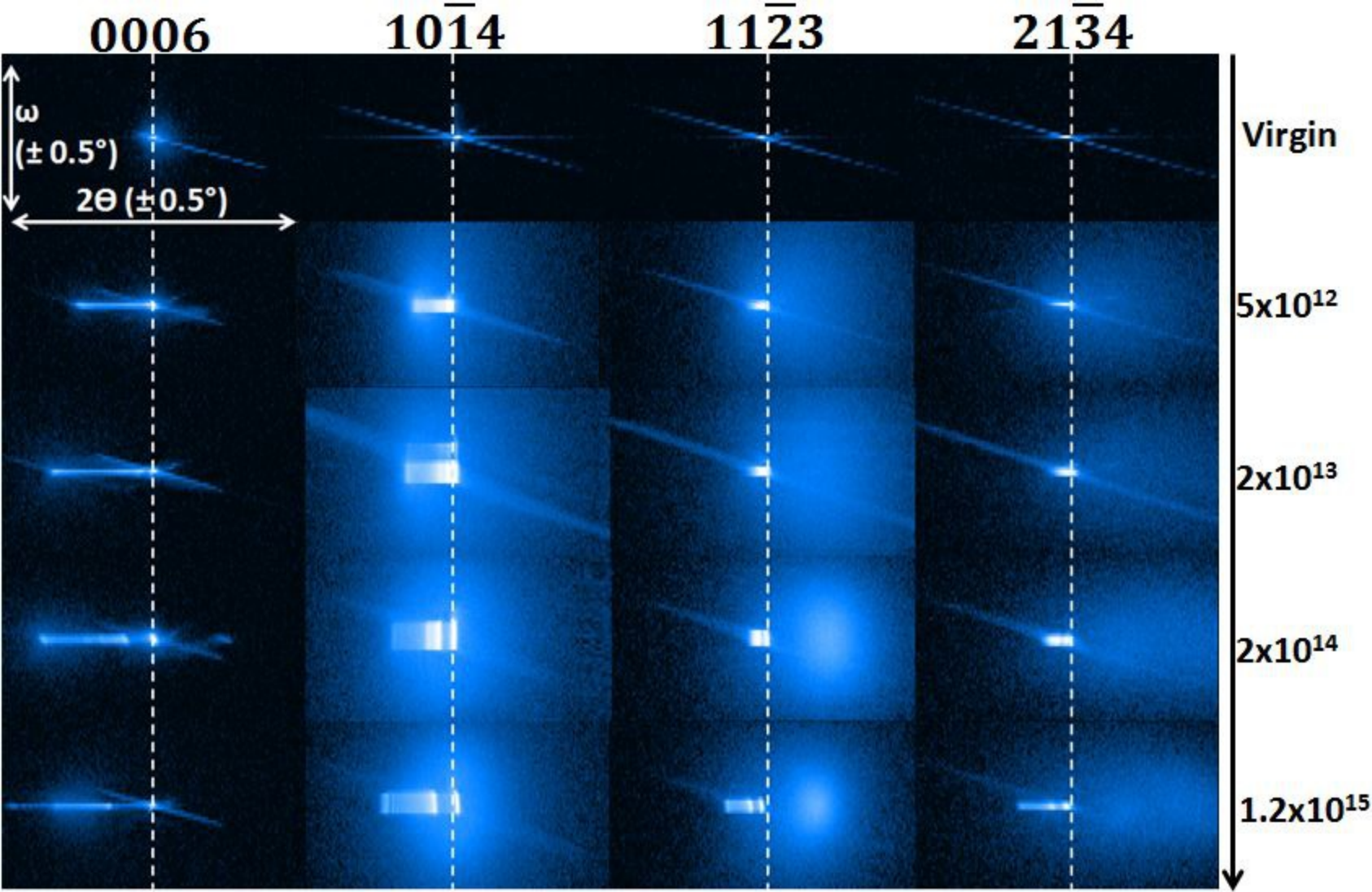
0006
10$\bar{1}$4
11$\bar{2}$3
21$\bar{3}$4
ω
(± 0.5°)
2θ (± 0.5°)
Virgin
5x10^12
2x10^13
2x10^14
1.2x10^15

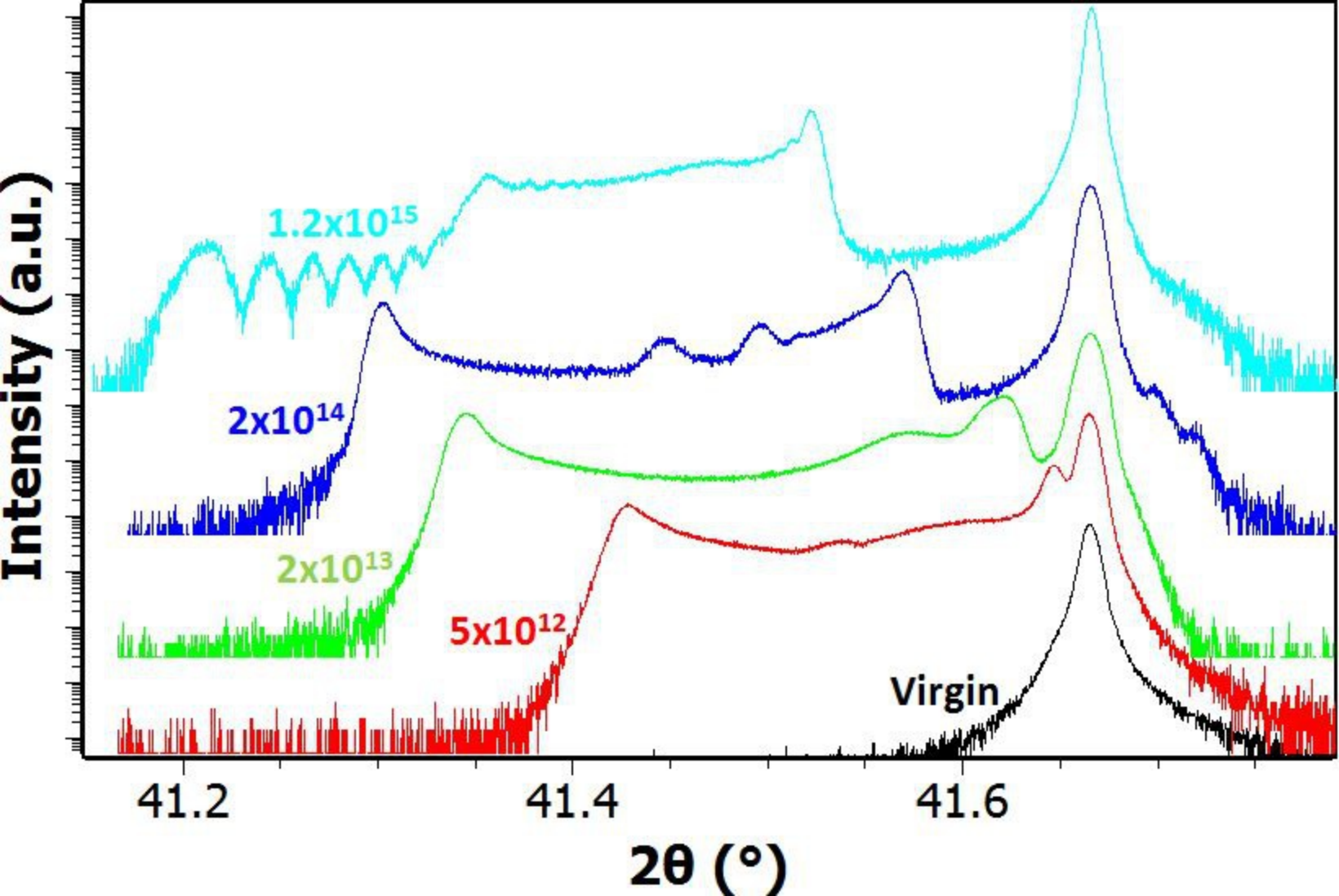
Intensity (a.u.)
1.2x10^15
2x10^14
2x10^13
5x10^12
Virgin
41.2
41.4
41.6
2θ (°)

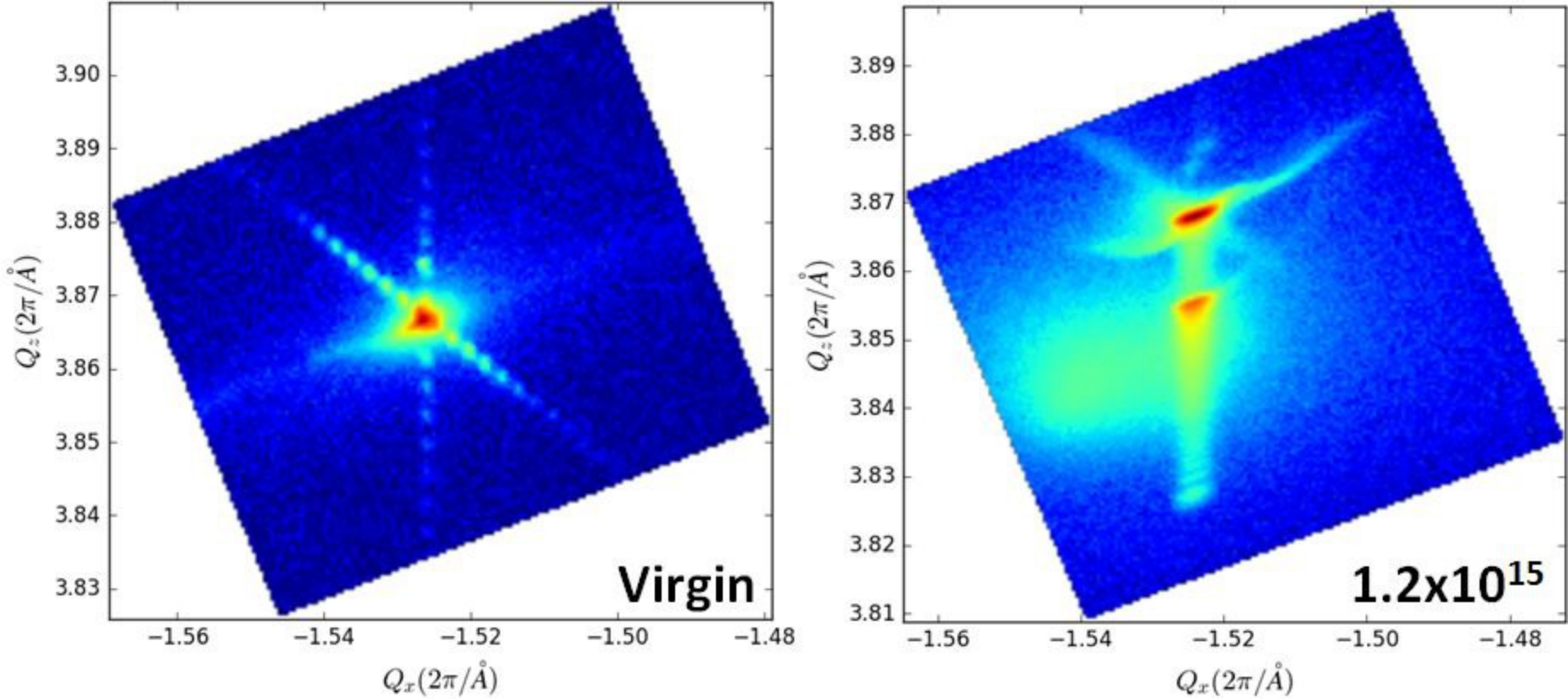
3.90
3.89
3.88
3.87
3.86
3.85
3.84
3.83
$Q_z(2\pi/\mathring{A})$
−1.56
−1.54
−1.52
−1.50
−1.48
$Q_x(2\pi/\mathring{A})$
Virgin
3.89
3.88
3.87
3.86
3.85
3.84
3.83
3.82
3.81
$Q_z(2\pi/\mathring{A})$
−1.56
−1.54
−1.52
−1.50
−1.48
$Q_x(2\pi/\mathring{A})$
1.2x10^{15}

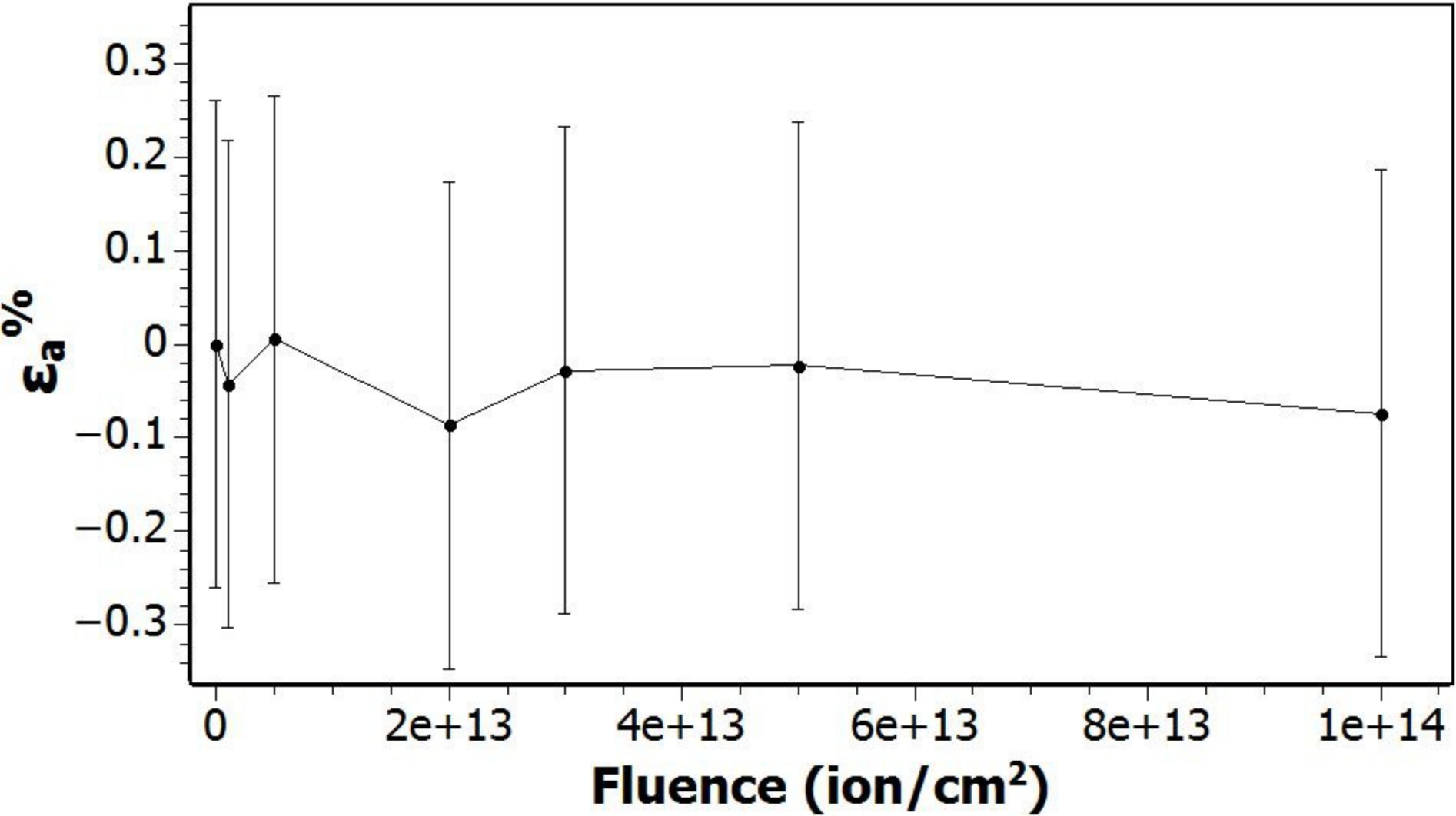
0.3
0.2
0.1
0
−0.1
−0.2
−0.3
ε_a %
0
2e+13
4e+13
6e+13
8e+13
1e+14
Fluence (ion/cm²)

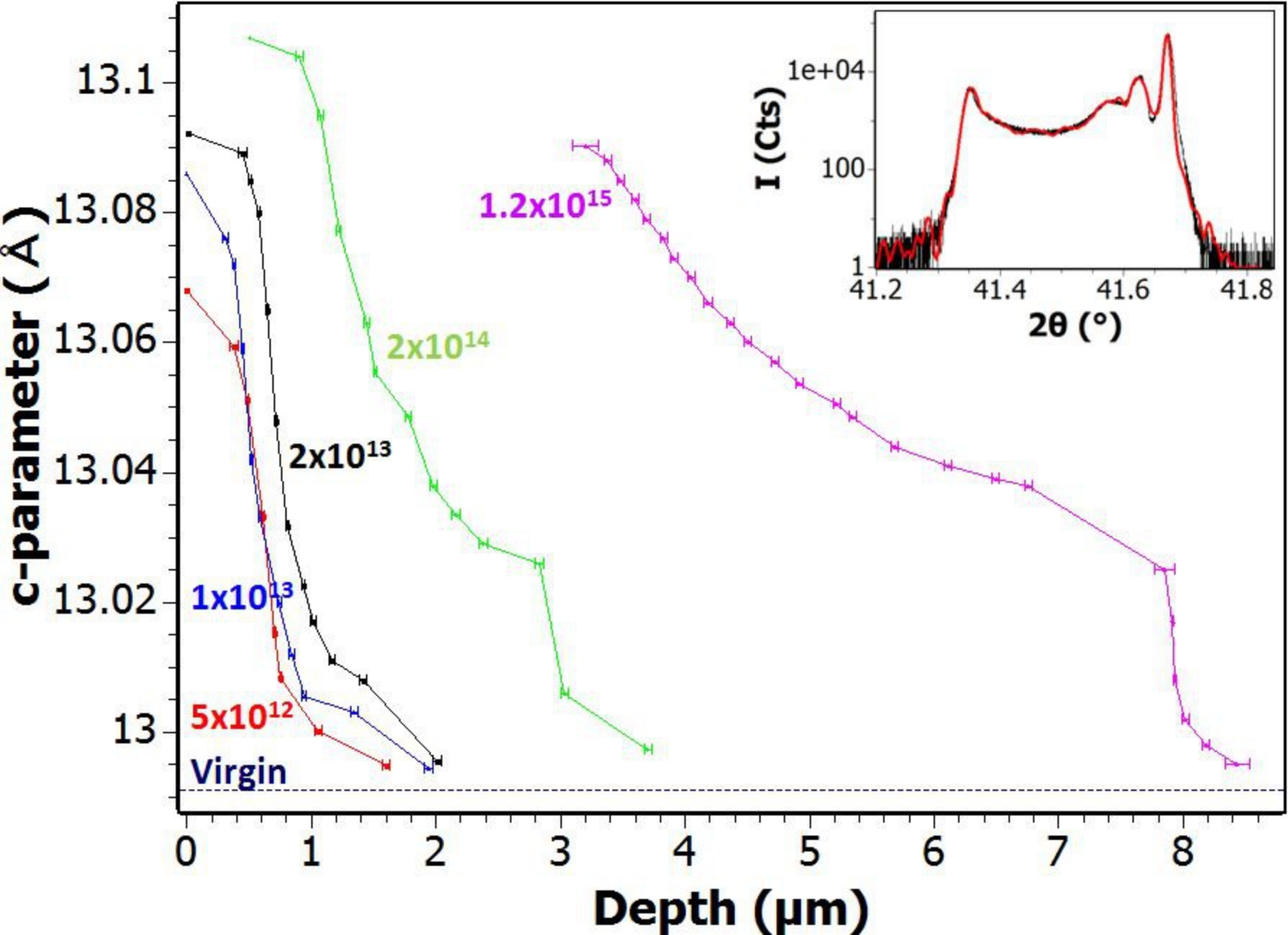
c-parameter (Å)
13.1
13.08
13.06
13.04
13.02
13
Depth (µm)
0
1
2
3
4
5
6
7
8
1.2x10^15
2x10^14
2x10^13
1x10^13
5x10^12
Virgin
I (Cts)
1e+04
100
1
41.2
41.4
41.6
41.8
2θ (°)

Reflections	2θ (°)	Chi (°)	Depth probed (μm)
0006	41.66	0	32.6
$10\bar{1}4$	35.14	39.1	27.6
$11\bar{2}3$	43.33	60.8	33.8
$21\bar{3}4$	66.50	64.3	50.2
$01\bar{1}8$(-)	61.28	0	24.2
$11\bar{2}0$	37.73	90	0.24